Ultrafast Laser Spectroscopy to Study Photodynamics of Asymmetric Hydrogenases

Amber Meyers,[1] Edwin J. Heilweil[2] and Christopher J. Stromberg[1]
[1]Department of Chemistry and Physics, Hood College, Frederick, MD 21701-8524, USA
[2] Physical Measurement Laboratory, National Institute of Standards and Technology (NIST), Gaithersburg, MD 20899, USA

Abstract

[FeFe]-hydrogenases are natural enzymes that catalyze the reduction of hydrogen. These enzymes, which contain iron in their active site, are of great interest because of the increasing need to develop less expensive substitutes for platinum commonly used as a catalyst for hydrogen production. Symmetric model compounds containing all CO ligands or mixed CO/CN and CO/PMe_3 ligands on the irons in the active site have been studied extensively. However, asymmetric compounds have not been the focus of much work. This study examines two asymmetric molecules containing both a single CN and five CO ligands: $[Fe_2(\mu\text{-}S_2C_3H_6)(CO)_5(CN)_1]^{1-}$ (**1**) and $[Fe2(\mu\text{-}S_2C_2H_4)(CO)_5(CN)_1]^{1-}$ (**2**) dissolved in room temperature acetonitrile. The asymmetry of these model compounds affects the redox potentials of the two iron atoms thus changing the catalytic properties of the compounds. These molecules were examined using femtosecond pulsed excitation with mid-infrared probe spectroscopy in order to better understand the ultrafast dynamics of the active site. Continuous ultraviolet lamp excitation with Fourier Transform infrared (FTIR) spectroscopy was also employed to explore stable product formation on the second timescale. For both model compounds, two timescales are observed; a 20-30 ps decay and formation of a long-lived product. The ps decay is assigned to vibrational cooling and rotational dynamics while the residual signal remains out to 300 ps suggesting new photoproducts are formed. A residual signal also remained out to the minute timescale, as observed using FTIR spectroscopy, but resulted in a different stable photoproduct

than observed on the ultrafast timescale. Density functional theory (DFT) calculations were used to simulate photoproducts for CO-loss and CN-loss isomers. The resulting photoproduct spectra suggest the picosecond transients arise from a complex mixture of isomerization after CO-loss. Other possibilities including dimerization and formation of a CN-containing Fe-CO-Fe bridging species are also considered.

Introduction

Hydrogen is a potential replacement for fossil fuels. Currently, hydrogen gas is generated from methane and fossil fuels, which industry is striving to move away from. For hydrogen to be a useful replacement for fuel, it must be generated more efficiently. In nature, hydrogen gas is produced very efficiently by bacteria from water in a slightly acidic environment. To do this, the microorganisms utilize hydrogenase enzymes to efficiently catalyze the reduction of protons to hydrogen gas.[1–9] Three types of hydrogenases exist in nature, the two most common being [NiFe]- and [FeFe]-hydrogenases. The [NiFe]-hydrogenases generally catalyze the oxidation of hydrogen gas into protons, whereas the [FeFe]-hydrogenases generally catalyze the reduction of protons to hydrogen gas.[3,4,6,9,10] The reduction of hydrogen ions into hydrogen gas is an essential step in producing hydrogen gas from water.

The active site of [FeFe]-hydrogenases contains a di-iron core with two bridging sulfur ligands and multiple pendant carboxyl (CO) and cyano (CN) ligands.[8,11–13] The general molecular structure of the native form [FeFe]-hydrogenase in one possible oxidation state is shown in Figure 1.[13] Many studies on small model compounds resembling the [FeFe]-hydrogenase active site have been completed, and although these synthesized model compounds

resemble the active site in structure, they are typically very poor catalysts on their own.[10,14–23] The simplest of these model compounds contains all CO ligands and is based on $Fe_2(\mu\text{-}S_2C_3H_6)(CO)_6$. Other model compounds are synthesized by making substitutions of the pendant CO ligands or by altering the carbon bridge between the two sulfurs.[15,23,24] Different pendant ligands alter the electronic properties of the active site and influence the catalytic properties of the molecule.[10]

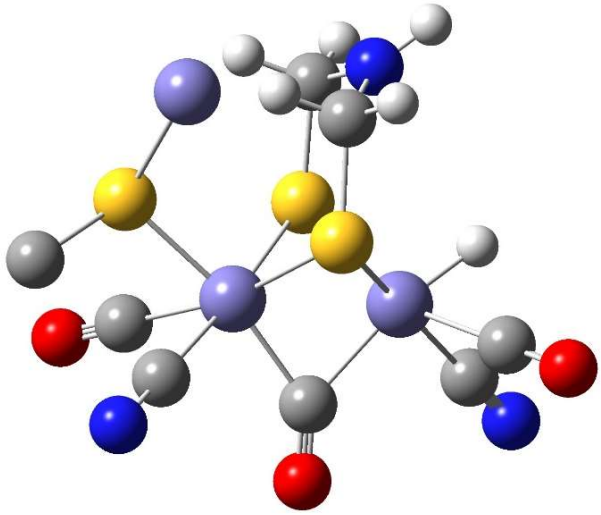

Figure 1. General form of the asymmetric active site of the native form [FeFe]-hydrogenase.[3,7,25–27]

Some model compounds have also been designed to use light to drive hydrogen gas production. One approach has been to bind the hydrogenases to elements of Photosystem I.[13,28,29] Another approach has been binding a photosensitizer to the hydrogenase. [30–41] In this approach, light absorbed by the photosensitizer would drive the redox reactions for hydrogen production, similar to the mechanism of Photosystem II.[33] However, the photodynamics of the [FeFe]-hydrogenase active site (and similar model compounds), especially on the ultrafast timescale are

not well understood. Symmetric model compounds containing all CO, mixed CO and CN, and mixed CO and PMe_3 ligands have been studied using ultraviolet (UV) or visible excitation with infrared (IR) probe spectroscopy.[42–46] However, asymmetric model compounds containing only one CN ligand, for example, have been synthesized but have not yet been investigated using TRIR spectroscopy.

In this work, the photodynamics of two asymmetric model compounds were studied at room temperature in acetonitrile solution: $[Fe_2(\mu\text{-}S_2C_3H_6)(CO)_5(CN)_1]^{1-}$ (**1**) and $[Fe2(\mu\text{-}S_2C_2H_4)(CO)_5(CN)_1]^{1-}$ (**2**). These molecules exist in different isomeric forms and the dominant isomeric structures of the studied compounds are shown in Figure 2. These model compounds exhibited a fast (20-30 ps decay) followed by a long-lived offset. Like symmetric model compounds containing two CN ligands, these molecules did not exhibit the fast (ca. 150 ps) decay previously observed in all CO or mixed CO/PMe_3 compounds, implying that the

asymmetry and inclusion of CN ligands could alter the catalytic capabilities of these model compounds.[43,44,47–50] Several DFT simulated spectra for CO-loss isomers show the possibility of a bridging Fe-CO-Fe species. The possible formation of a bridging Fe-CO-Fe species could also affect the catalytic properties of the molecule.

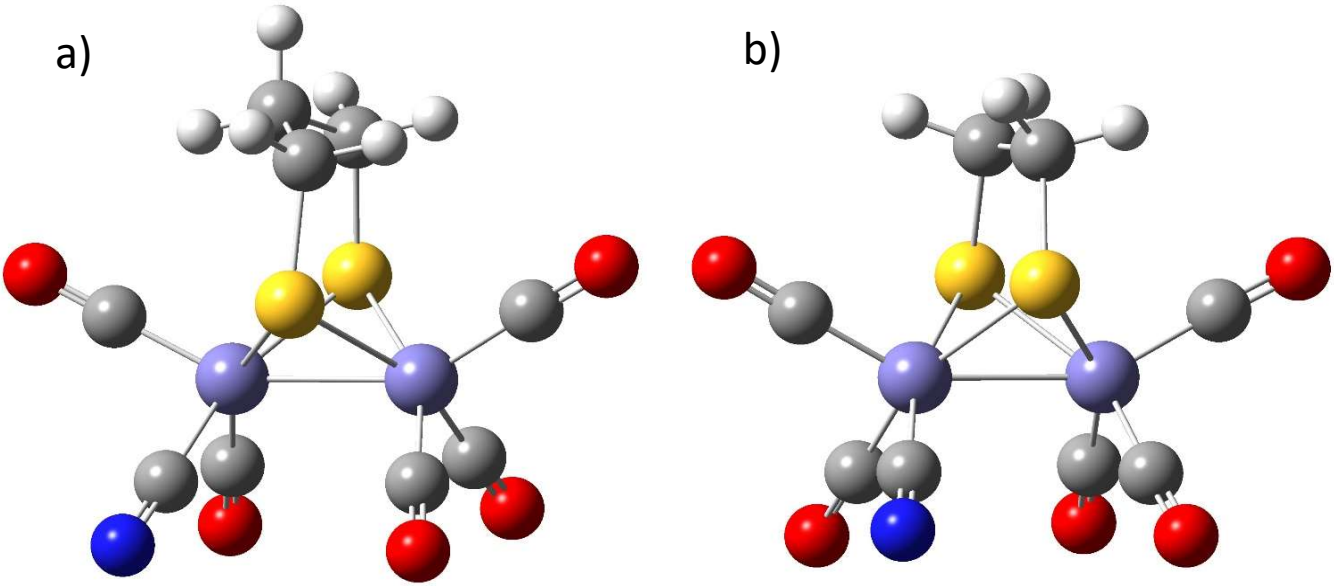

Figure 2. Structure of (a) an axial isomer of $[Fe_2(\mu\text{-}S_2C_3H_6)(CO)_5(CN)_1]^{1-}$ and (b) an axial isomer of $[Fe_2(\mu\text{-}S_2C_2H_4)(CO)_5(CN)_1]^{1-}$.

Methods

Synthesis. Syntheses of **1** and **2** have been previously published.[15] The synthesis of **1** is summarized as follows: previously synthesized[15] $Fe_2(\mu\text{-}S_2C_3H_6)(CO)_6$ was combined with $ONMe_3{\cdot}2H_2O$ and acetonitrile (MeCN) under nitrogen atmosphere. The solution was cooled to −40 °C. One equivalent of Et_4NCN was combined with MeCN under nitrogen atmosphere and

added to the cold flask. The reaction mixture warmed to room temperature for 2 hours, and then the solution evaporated to dryness under vacuum. The remaining dark red oil was extracted into tetrahydrofuran and filtered. The volume was reduced under vacuum and the product was precipitated upon washing with hexanes and evaporated to dryness. Purity of the product was checked using FTIR. Synthesis of **2** is similar, except starting with $Fe_2(\mu\text{-}S_2C_2H_4)(CO)_6$.

Time Resolved UV-Pump/IR-Probe Laser Spectroscopy. A 40 fs Ti:sapphire oscillator tuned to 800 nm seeded a home-built Ti:sapphire regenerative amplifier. The regenerative amplifier produced 800 nm, 80 fs, 700 μJ pulses at a frequency of 1 kHz. These pulses were used to pump a Spectra-Physics OPA-800F optical parametric amplifier (OPA).[51] The OPA produced signal and reference pulses, which were difference frequency mixed in a AgGaS crystal resulting in 120 fs, ~1 μJ pulses in the mid-IR centered around 2000 cm^{-1} (CO-stretching region) with a bandwidth of ca. 230 cm^{-1} full-width at half-maximum (FWHM). Residual 800 nm light from the OPA was either doubled (400 nm) or tripled (266 nm) to produce excitation pulses.

The pump and probe beams were overlapped and transmitted through a flow cell with 2 mm pathlength and CaF_2 windows. Samples of **1** and **2** were prepared in anhydrous MeCN at ca. 10^{-3} M concentration to achieve optical densities (OD) of approximately 0.8 for IR peak absorptions. The timing of the probe pulses relative to the pump pulses was adjusted using a computer-controlled optical delay stage with a maximum delay time of 300 ps. The IR beam traversed a 50% beamsplitter so that the second IR beam is also directed through the sample cell separated from the pump beam and used as a reference to normalize the IR probe signal. The pump beam was chopped at 500 Hz to allow iterative collection of excited versus unexcited sample transmission.

The transmitted IR signal and reference beams were passed through a scanning grating monochromator with 4 cm^{-1} FWHM resolution and imaged onto a matched pair of Mercury-Cadmium-Telluride (MCT) detectors. The detector pre-amplified outputs for each laser pulse were sampled by boxcar averagers and analog-to-digital converters. Collected signals were processed by home-built software to extract the averaged pump-induced differential optical density (ΔOD) at each wavelength as the monochromator is scanned across the spectrum.

Two types of ultrafast time-resolved IR (TRIR) scans were conducted. First, entire spectral scans were obtained at various time-delays. Two separate runs for each delay time were averaged to obtain better signal-to-noise (with approximately ±0.002 OD). From these spectra, wavelengths of importance were strategically chosen. Kinetic scans were then obtained at these wavelengths with pump-probe delay time scanned from -35 ps to 285 ps with a resolution of approximately 2 ps. Higher resolution scans were also taken around t=0 with delay time ranging from -8 ps to 25 ps with resolution of approximately 0.2 ps.

Long Delay Time FTIR Spectroscopy. Samples were loaded into a static 1.0 mm pathlength IR cell fitted with CaF_2 windows and placed in a dry-air and carbon dioxide purged Nicolet Magna 550 FTIR spectrometer.[51] The sample was exposed to UV light from a broad-band mercury pen lamp for 30 s intervals. IR spectra were taken at the beginning and after each interval of UV exposure. Difference spectra were calculated for each interval of UV exposure by dividing spectra not exposed to UV by spectra that had been exposed to UV. This process permits identification of starting molecule loss and formation of new product species by new IR absorption features.

DFT Calculations. DFT-predicted IR spectra were calculated using Gaussian 09W.[52,53] Gas-phase calculations were performed using the BP86 functional[54–56] with the TZVP basis set,[57,58]

which has performed well for related model compound studies.[42–46] While absolute frequency agreement between DFT results and experiments is generally found to be poor, relative frequency shifts and amplitudes adequately agree to make favorable product and intermediate structural assignments.[30-34] Calculated infrared "stick" spectra were convolved with a 15 cm^{-1} FWHM Lorentzian function to mimic features broadened by MeCN solvent. Calculations were performed for each isomer of **1** and **2** and for all possible CO- and CN-loss photoproduct fragments that could result from UV excitation. The ground state and CO-loss isomers for **1** and **2** are shown in Figures 3 and 4, respectively.

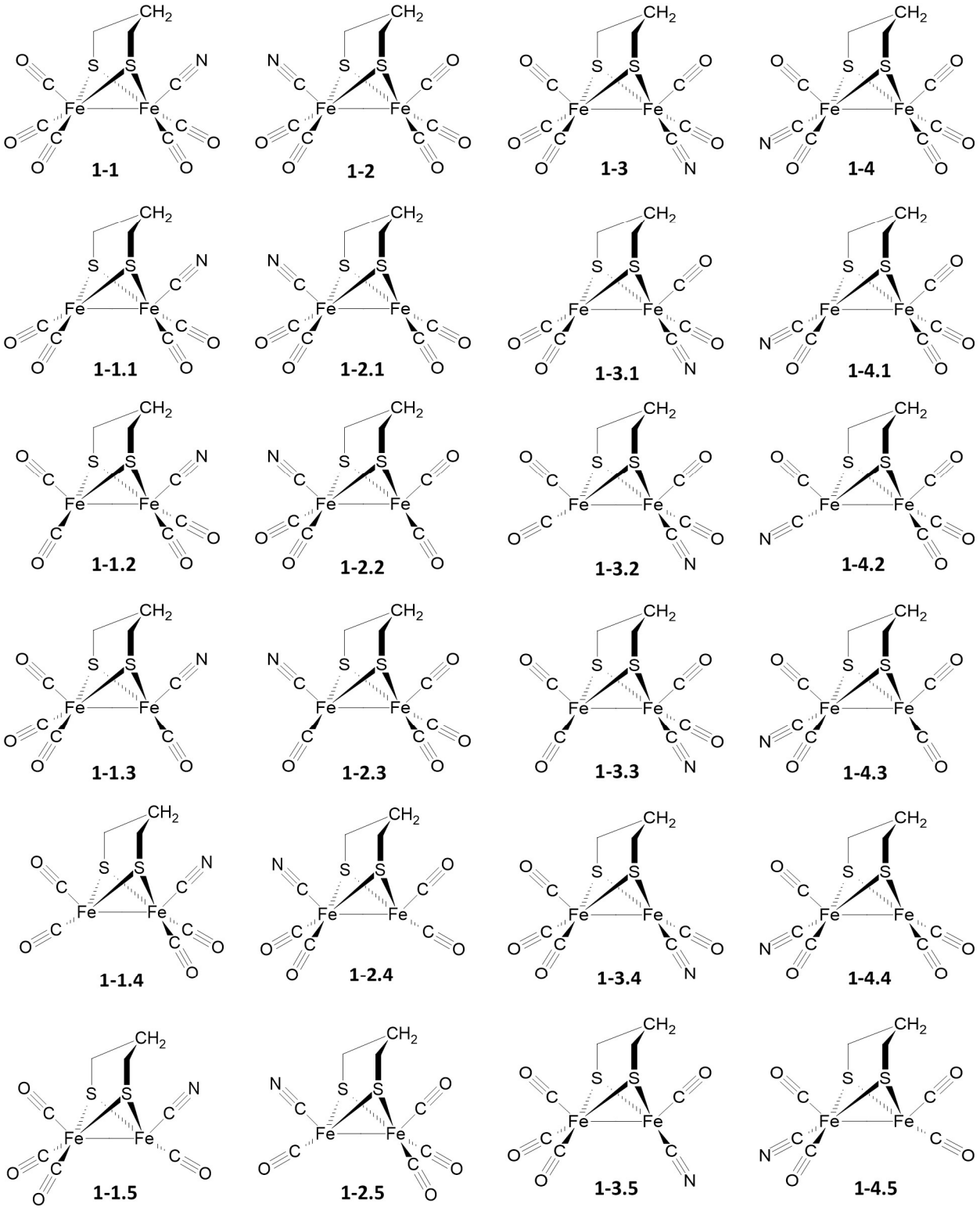

Figure 3. Ground state and CO-loss isomers for **1**.

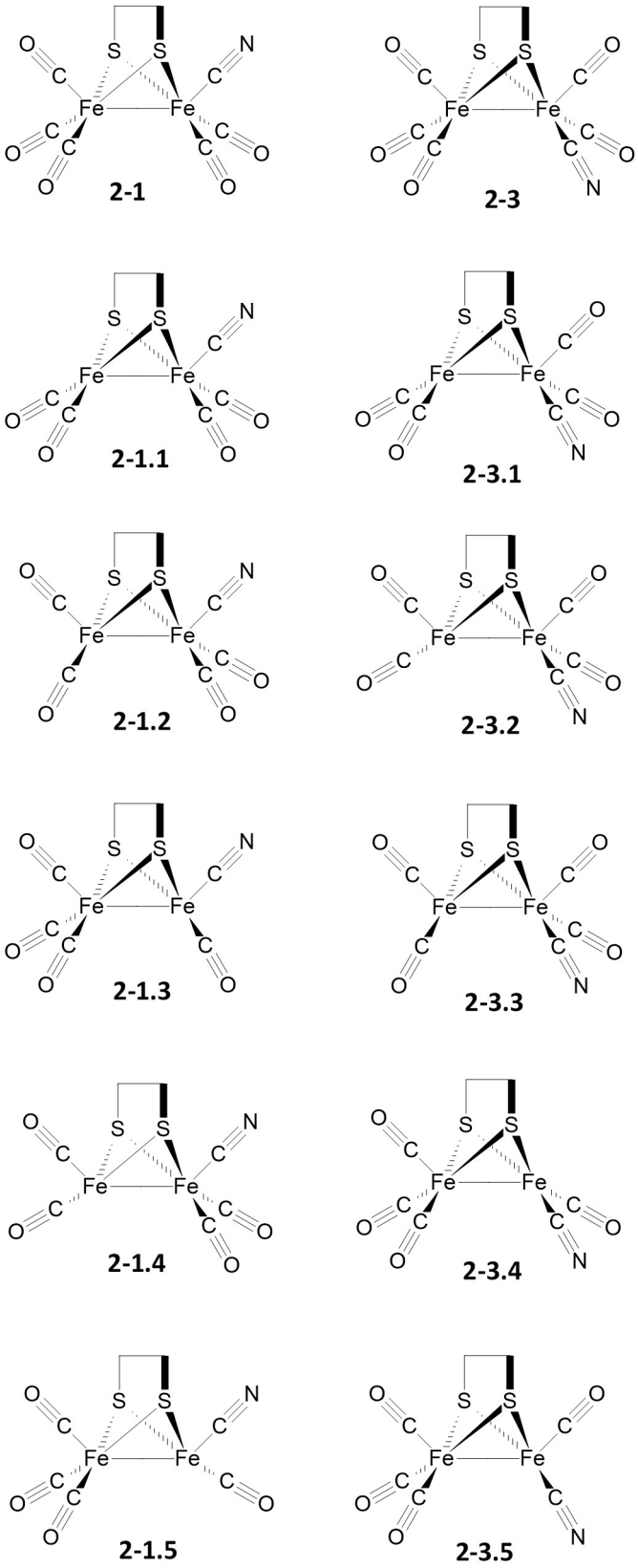

Figure 4. Ground state and CO-loss isomers for **2**.

Results and Discussion

Steady State Spectra

1 can exist as four possible isomers. Isomers **1-1** and **1-2** (as well as **1-3** and **1-4**) differ only by the direction the bridge points. For these compounds, as with others studied[42,44,46], the bridge flip isomeric forms do not significantly affect room temperature vibrational spectra. Compound **2** can exist as two possible isomers as the compound is ethyl-bridged and does not have a bridge flip (these are numbered **2-1** and **2-3**, for consistency with **1**).

The FTIR ground state spectrum for compound **1** (Figure 5a), displays distinct CO-stretching band absorptions at 1914 cm^{-1}, 1976 cm^{-1}, and 2030 cm^{-1}. There is also a wide band centered around 1950 cm^{-1} that is the result of at least two overlapping CO-stretching absorptions. The weaker CN-stretching band is located at 2092 cm^{-1}. IR spectra for each isomer of **1** were calculated using DFT methods. Results of these calculations are shown in Figure 5b. Note that the spectra of **1-1** and **1-2** are nearly identical, while the spectra of **1-3** and **1-4** are indistinguishable. There is a shift in the scale of the calculated spectra, which causes the calculated spectra to look more compressed than the experimental spectra.

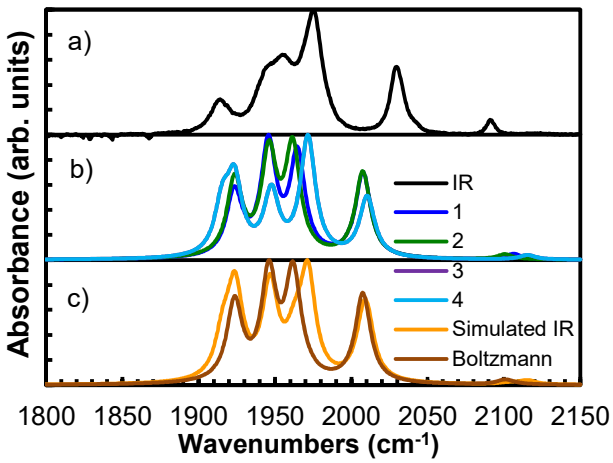

Figure 5. (a) Experimental IR spectrum of **1** in room temperature acetonitrile, (b) Simulated IR spectra for each ground state isomer of **1** based on DFT calculations, (c) comparison of simulated

IR spectra assuming a Boltzmann distribution of isomers (brown) and a mixture of 70% of isomer **1-3** and 30% isomer **1-1** (orange).

By comparing simulated FTIR spectra of the possible isomers (via DFT calculations) with the spectra of the synthesized sample, the isomers and their relative amounts present in the sample can be determined. None of the simulated spectra on their own match the experimental spectra exactly, which indicates that a mixture of CN-containing isomers was initially synthesized. If only isomers **1-3** and/or **1-4** were present in solution, only one distinct, weaker band at a lower frequency from the strongest band would be observed, instead of the broad overlapping bands in the experimental spectrum. If only isomers **1-1** and/or **1-2** were present in solution, the experimental spectra would not show the strongest band near 1976 cm^{-1}. Since the experimental spectrum cannot be explained by the simulated spectra of a single isomer, a mixture of isomers was considered. The strong band in the experimental spectrum at 1976 cm^{-1} that is only seen in isomers **1-3** and **1-4** indicates that they are the predominant isomers in solution. The broad band to the left of the strong band in the experimental spectrum is likely composed of at least two overlapping bands. Since it is not a distinct peak, which would be the case if only isomers **1-3** and/or **1-4** were present, isomers **1-1** and/or **1-2** must be present as well. A mixture of isomers was simulated as shown in Figure 5c. We conclude there is approximately a 70:30 ratio in abundance of isomers **1-3** and/or **1-4** to isomers **1-1** and/or **1-2.** The ratio of isomers may be closer to 60:40 or 80:20, but isomers **1-3** and/or **1-4** are clearly dominant. As was found for other compounds, isomers **1-3** and **1-4** are the most polar isomers and are likely stabilized by being in acetonitrile solution. This would explain why they are present in higher abundance than isomers **1-1** and **1-2**, which are less polar and are the lowest energy isomers in gas phase calculations.

Time Resolved UV-Pump/IR-Probe Laser Spectroscopy

Compound 1 in MeCN. Ultrafast TRIR was used to collect scans at different pump-probe time delays using 400 nm pump. The data are shown in Figure 6 for **1**. Additional data was collected for **1** using both 266 nm and 400 nm pump wavelengths (Figure 7), which generated qualitatively very similar spectral difference data. Any apparent differences are due to a small calibration drift and because the data sets were taken at different times. The analysis below is based on the data shown in Figure 6, although the same conclusions result from a detailed analysis of the data in Figure 7, as well. Parent species loss (bleaches) occurs below the baseline and new product absorptions are above the baseline. Bleaches are seen for **1** at 1930 cm^{-1}, 1979 cm^{-1}, and 2036 cm^{-1}. These bleaches generally correspond well with FTIR absorptions, except for around 1956 cm^{-1}, where there is an absorption in the FTIR spectra, but very little signal in the TRIR spectra. At this spectral position, there is likely a new absorption that overlaps the bleach that would be expected there, resulting in cancellation of the bleach. New absorptions are observed for photoexcited **1** at 1963 cm^{-1}, and 2038 cm^{-1} out to 300 ps delay time. A weak new absorption feature may also be present around 1900 cm^{-1} (this is more clearly seen in the data in Figure 7).

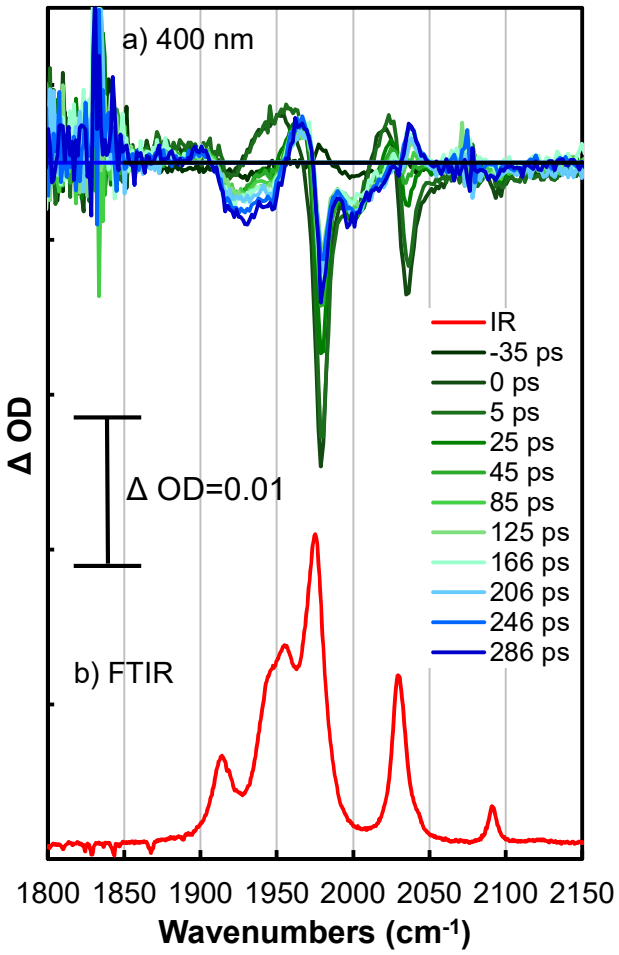

Figure 6. Time-resolved UV and visible pump, IR probe spectra for **1** in acetonitrile at indicated time delays after excitation with (a) 400 nm, and (b) ground-state FT-IR spectrum of **1** in acetonitrile solution.

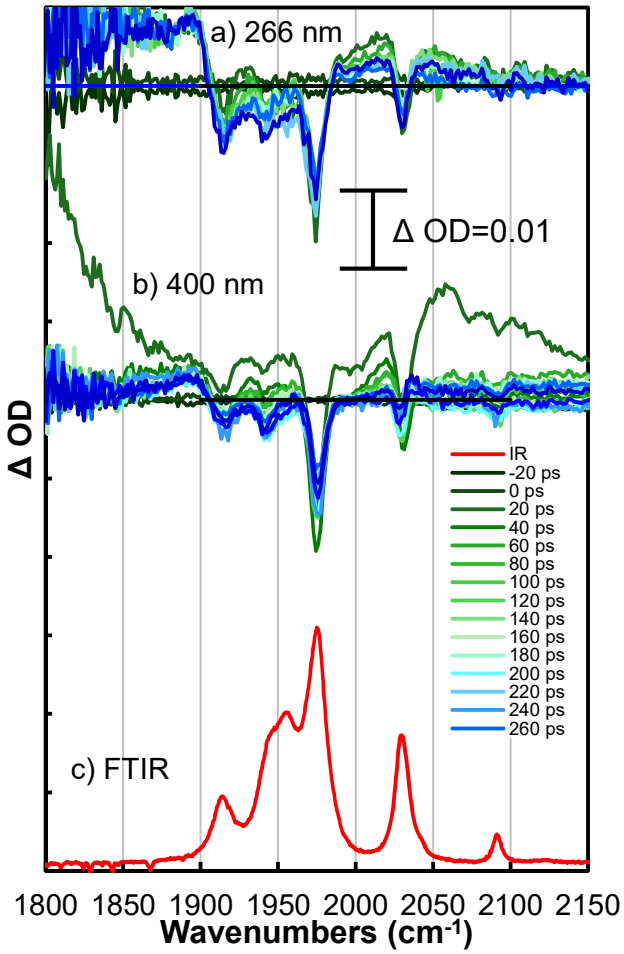

Figure 7. Time-resolved UV and visible pump, IR probe spectra for **1** in acetonitrile at indicated time delays after excitation with (a) 266 nm and (b) 400 nm, and (c) ground-state FT-IR spectrum of **1** in acetonitrile solution.

The difference frequency spectral scans were examined to select wavenumbers associated with bleach and new absorption features to perform dynamical measurements. Time-delay scans were taken at these wavenumbers at high and low time-step densities in order to better understand the dynamics of the bleaches or absorptions at those wavenumbers. The raw time-delay scans for **1** at the noted wavenumber positions are shown in Figure 8a. In all cases, an instrument-limited risetime at delay time t=0 is observed followed by a rapid intensity decrease and flat offset. Two different time scales are extracted from the time-delay scans for each

compound using a simple single exponential fit with offset model. These fits are complicated by new absorptions that nearly cancel out the bleaches entirely. The fits for two dynamical scans are shown for **1** in Figures 8b and 8c. For **1** a rapid 23 ± 6 ps decay is observed followed by a long-lived offset.

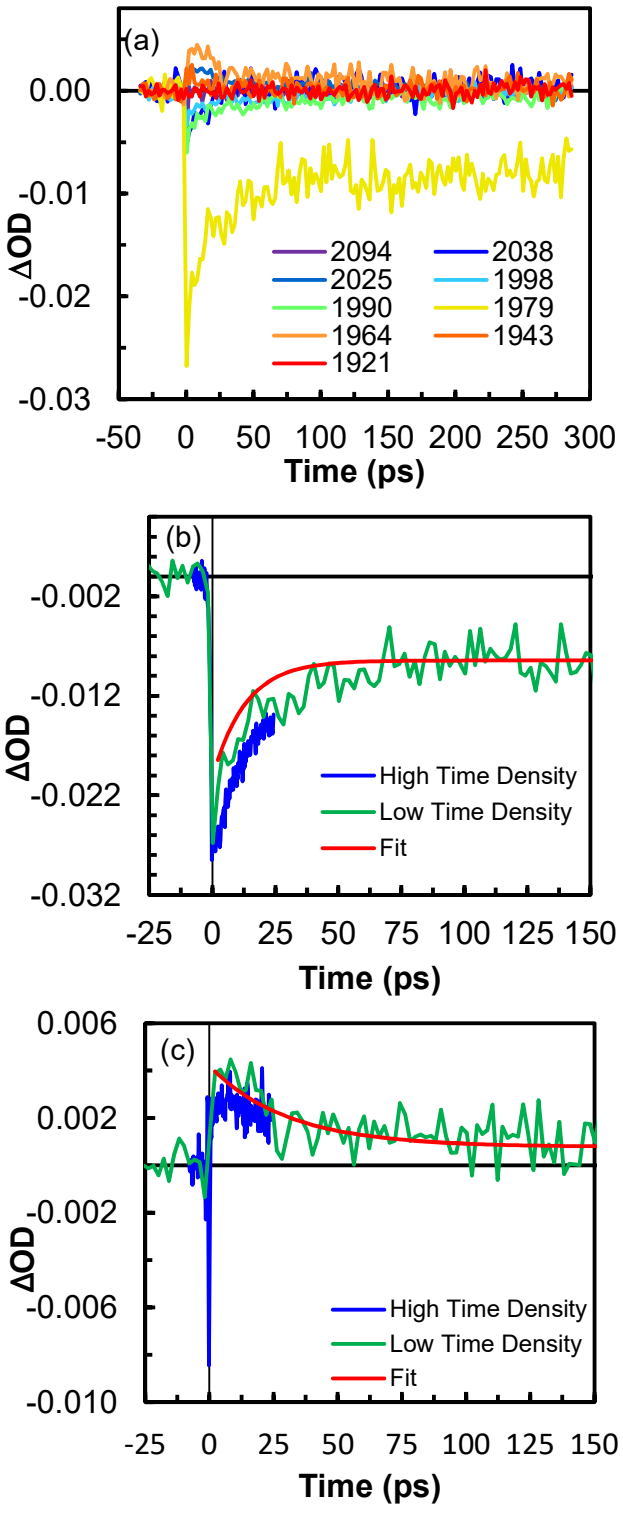

Figure 8. Time-dependent scans for **1** in acetonitrile using 400 nm pump at (a) all selected wavenumbers, (b) 1979 cm^{-1}, (c) 1964 cm^{-1}.

The 20-30 ps decay is likely due to vibrational cooling of possible photoproducts resulting from relaxation of the excited state.[47,49,50] This behavior is especially noticeable at ~1950 cm^{-1} and ~2021 cm^{-1}, where the short time spectra are broad and shifted to lower wavenumbers, indicative of anharmonic overtone absorption from coupled hot bands to CO-stretching vibrations. After approximately 20-30 ps, the molecule returns to the ground vibrational state. The intermediate spectra "relax" to the long-time spectrum, which is narrower and shifted to higher wavenumbers. Evidence of vibrational cooling has been observed in previously examined related molecules[42,43], but not as distinctly as in **1** and **2.** There are also likely rotational dynamics contributing to the early-time spectra, as observed in other similar model compounds,[59–61] in addition to the vibrational dynamics. The long-lived spectrum at ~300 ps delay suggests that new photoproducts are formed that may be stable with ns or longer lifespans.

In order to better locate and represent new absorption features for the long-time delay photoproduct without overlapping bleaching features, the ground state IR spectrum for **1** was added to the longest time-delayed spectrum obtained (at 286 ps, dark blue in Figure 6)**,** as shown in Figure 9. In order to account for the difference in intensities between the TRIR spectrum and the FTIR spectrum, a multiplying normalization factor was applied to the product spectrum. This multiplicative factor was approximated by eye and adjusted in order to minimize the negative absorption at ~1928 cm^{-1}. It was not possible to minimize both of the negative absorptions at ~1928 cm^{-1} and ~2000 cm^{-1}. These negatively absorbing features in the product spectrum are due to a broadening in the TRIR spectrum that is not observed in the FTIR spectrum. Using this analysis, the absorption at 1916 cm^{-1} can be seen to have shifted to the red (lower wavenumber)

of the absorption of the starting molecule. The absorption at 1963 cm^{-1} has also shifted to the red, but the absorption at 2033 cm^{-1} has shifted very slightly to the blue (higher wavenumber).

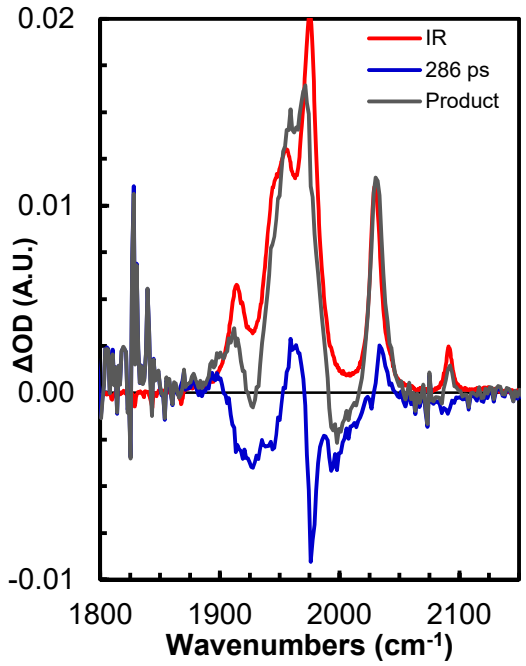

Figure 9. Long time-delay product spectrum extrapolated from the 286 ps delay and FTIR spectra for **1.**

In order to identify the product structure, the possibility of isomerization upon excitation or relaxation to the ground state was considered, since it was previously observed in related di-iron model compounds.[42,44,47] In this case the possibility of isomerization alone can be ruled out by comparing the observed shifts to the expected shifts that would occur due to isomerization. For example, assuming there is approximately a 70:30 isomer ratio as previously described, all of **1-1** and/or **1-2** could potentially isomerize to **1-3** and/or **1-4** upon excitation. If this were the case, the absorption at 1903 cm^{-1} would shift to the red while the absorptions at 1961 cm^{-1} and 2033 cm^{-1} would be expected to shift considerably to the blue (Figure 5b). Since the observed shift is to the red at 1961 cm^{-1} the possibility of **1-1** and/or **1-2** isomerizing completely to **1-3** and/or **1-4** can be ruled out. Using a similar analysis, the possibility of **1-3** and/or **1-4**

isomerizing to **1-1** and/or **1-2** can also be ruled out. In that case, a blue shift at 1900 cm^{-1} and red shifts at 1961 cm^{-1} and 2033 cm^{-1} would be expected, which is not observed experimentally.

Another possibility would be loss of the CN ligand upon UV excitation. To address this possibility, DFT calculations were performed to simulate the spectra of all possible CN-loss isomers, shown for **1** in Figure 10a. A CN-loss would result in a significant shift to the blue of all CO-stretching bands, which is not observed in the product spectrum. The possibility of CN ligand loss is ruled out entirely.

Another possibility is loss of a CO ligand upon UV excitation. DFT calculations were performed to simulate all CO-loss isomers, shown for **1** in Figure 10b-e. Several CO-loss isomers match the observed shifts to the red at 1900cm^{-1} and 1961 cm^{-1}. However, not a single CO-loss isomer is expected to result in a blue shift at 2033 cm^{-1}, which was observed experimentally, so the loss of a CO ligand alone can also be ruled out.

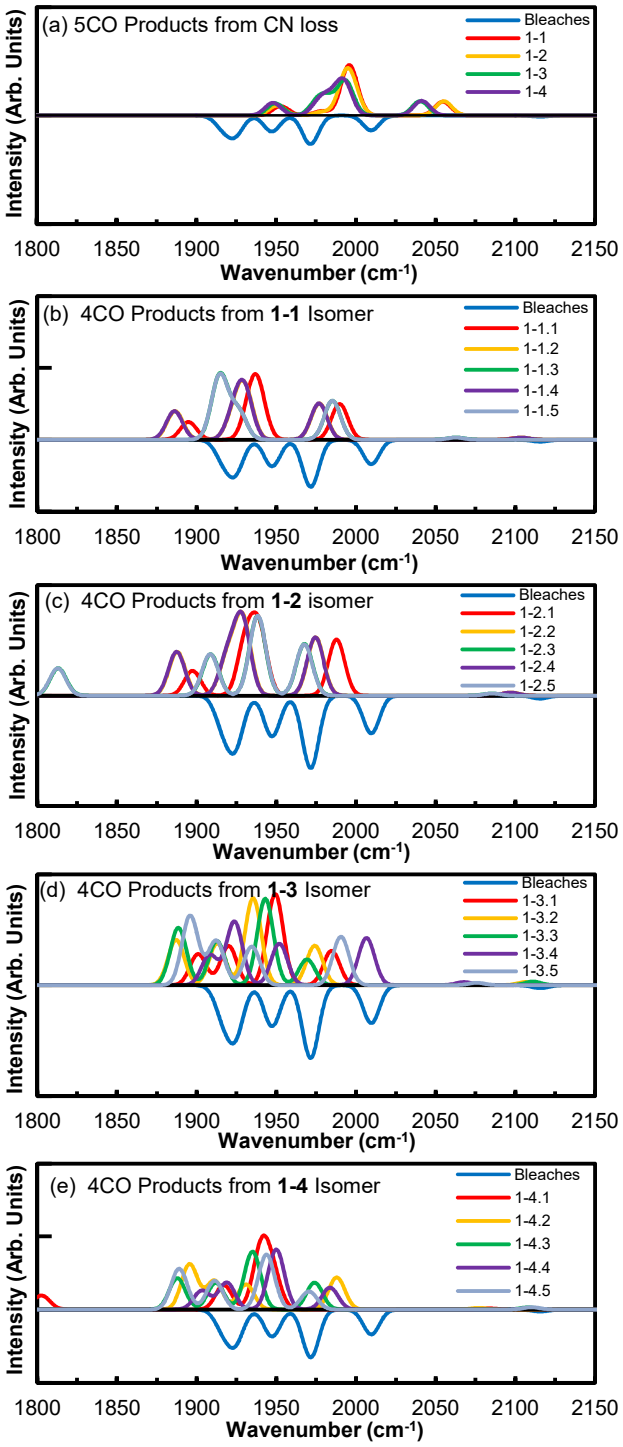

Figure 10. Calculated DFT spectra for all CO and CN-loss photoproduct isomers of **1**: (a) CN-loss isomers and (b-e) CO-loss isomers originating from possible ground state isomeric structures. Isomers that differ only by the direction the bridge points typically have identical spectra and may be indistinguishable.

Since isomerization and ligand-loss alone do not explain the spectrum of the photoproduct, it is likely that the observed shifts are due to some complex mixture of isomerization and CO-loss. For example, the only possibility that would result in the observed blue shift at 2033 cm^{-1} is isomerization of **1-1/1-2** to **1-3/1-4**. This isomerization, combined with a CO-loss would match the red shifts at 1900 cm^{-1} and 1961 cm^{-1}, as well at the blue shift at 2033 cm^{-1}. Other, more complicated explanations also exist, such as dimerization, which would be difficult to model or test with any certainty, or formation of a bridging Fe-CO-Fe species.

It is possible that a CO-loss photoproduct would form a bridging Fe-CO-Fe species. In particular, isomers **1-2.3, 1-2.5,** and **1-4.1** all show evidence of a bridging CO bond (Figures 10c and 10e). Unfortunately, we did not acquire TRIR spectral data in the bridging CO-stretching region (~1800 cm^{-1}) and are unable to conclude whether or not a bridging CO is observed. However, we can conclude that a bridging CO isomer alone does not explain the product spectrum. If a bridging CO species were to be formed, the spectrum of the product would be shifted significantly to the red, which is not observed.

Additionally, DFT calculations show that the bridging CO isomers have smaller dipoles than other isomers in that same isomer "family". The use of acetonitrile, a very polar solvent, makes it unlikely that these bridging CO isomers with small dipoles would be formed over other isomers with larger dipoles.

Compound 2 in MeCN. Ultrafast TRIR was used to collect spectral scans at different time delays using 400 nm excitation for **2** (Figure 11). Similar results as **1** were observed for **2.** Time delay scans were taken for **2** (Figure 12a) and the fits for some of these scans are shown in Figure 12b and c. Two timescales were observed for **2**; a 25 ± 9 ps decay, followed by a long-

lived offset. As was done for **1** in order to see the locations of new absorptions, the long-time TRIR spectra for **2** was added to the FTIR ground-state spectrum for **2** (Figure 13) and the same analysis of comparing shifts as was performed for **1** was applied. Product spectra were compared to DFT simulated spectra for different possible isomeric structures (see Figure 14).

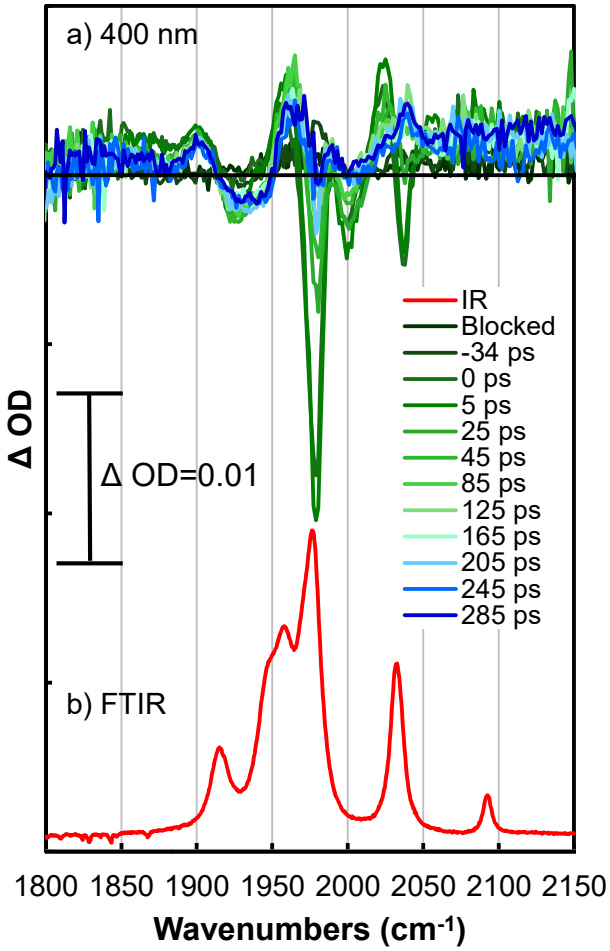

Figure 11. Time-resolved UV and visible pump, IR probe spectra for **2** in acetonitrile at indicated time delays after excitation with (a) 400 nm, (b) ground-state FT-IR spectrum of **2** in room temperature acetonitrile solution.

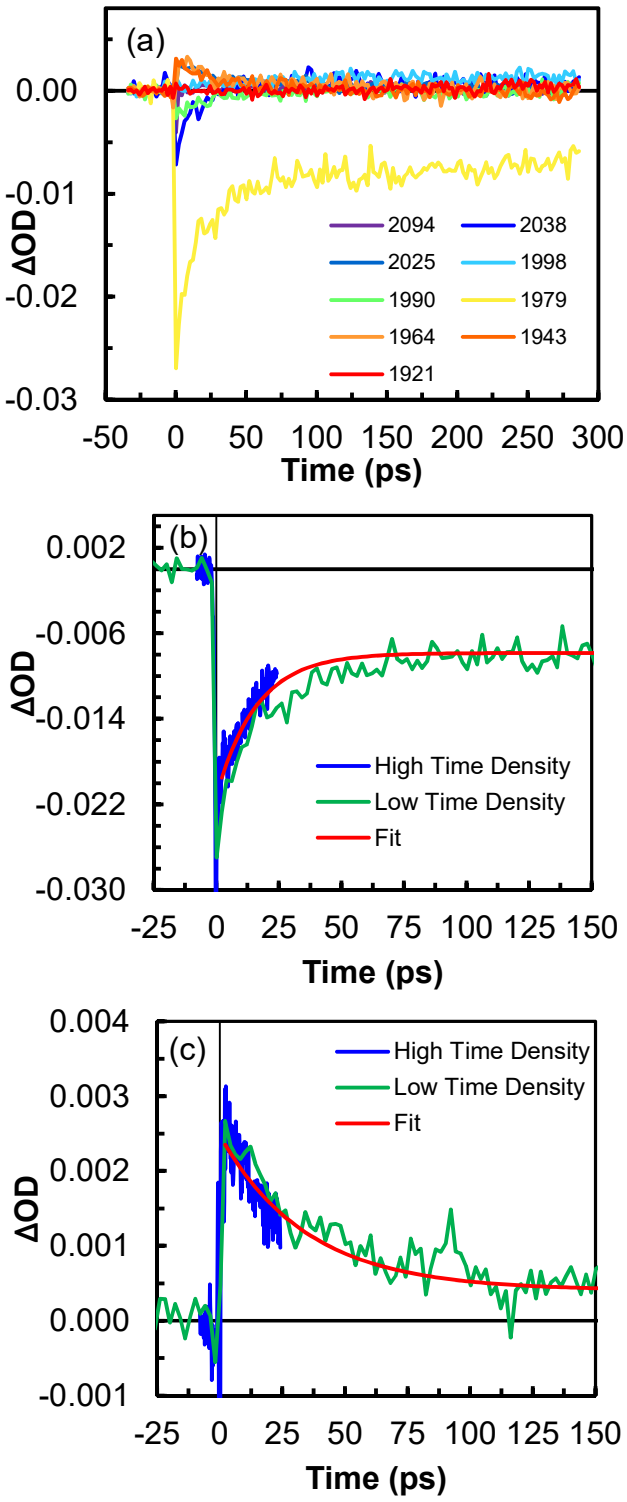

Figure 12. Time-dependent scans for **2** in acetonitrile using 400 nm pump at (a) all selected wavenumbers, (b) 1979 cm^{-1}, (c) 2023 cm^{-1}.

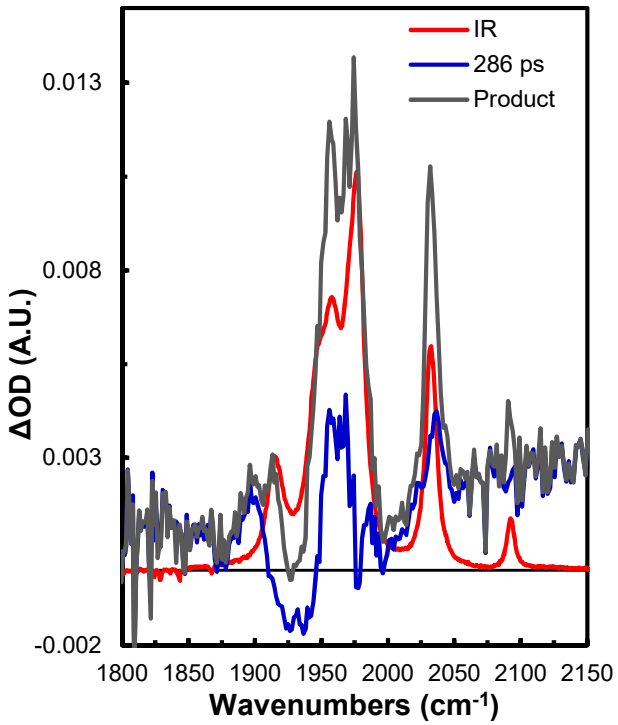

Figure 13: Long time-delay product spectrum extrapolated from the 286 ps delay and FTIR spectra for **2.**

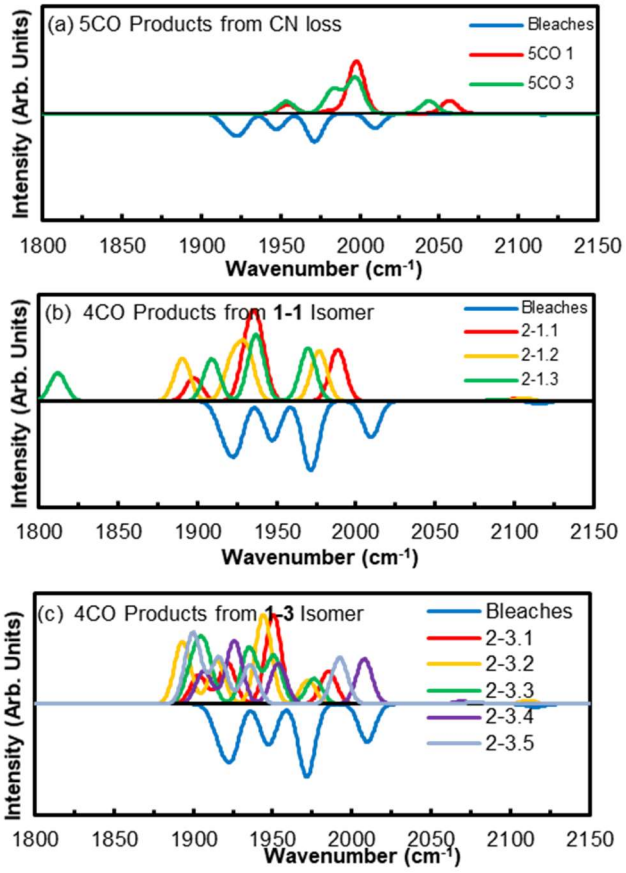

Figure 14: Calculated DFT spectra for all CO and CN-loss photoproduct isomers of **2**: (a) CN-loss isomers and (b,c) CO-loss isomers originating from possible ground state isomeric structures.

Long Time-Delay FTIR Spectroscopy:

Minute timescale IR difference spectra for **1** and **2** are shown in Figures 15 and 16, respectively. The longest time spectra for each compound was added to its corresponding ground-state FTIR spectrum so that the locations of new absorptions would be easier to identify, as shown in Figures 17 and 18. For **1**, new absorptions are observed at 1905 cm^{-1}, 1941 cm^{-1}, 1978 cm^{-1}, and 2086 cm^{-1}. The absorption at 1905 cm^{-1} shifted to the blue while the absorptions at 1941 cm^{-1} and 1987 cm^{-1} shifted considerably toward the red. The weak CN-stretch absorption at 2086 cm^{-1},

which was indistinguishable from the noise in the TRIR data, remains in the spectrum but is observed to shift slightly to the red. These shifts were compared to those observed in the TRIR data. The directions of the shifts at corresponding wavelengths between FTIR and TRIR data do not match. Recall that in the TRIR data, the absorption around 1900 cm^{-1} shifted to the red, whereas that absorption shifts to the blue in the FTIR spectra. This implies that different photoproducts are formed on the second timescale rather than on the picosecond timescale. The large red-shift of the absorptions at 1941 cm^{-1} and 1987 cm^{-1} suggest that a stable CO-loss photoproducts are formed (Figure 10). This is surprising because we would not expect a 4-CO photoproduct to be stable on the minute timescale because CO is expected to recombine within microseconds at millimolar concentrations of the starting compound.

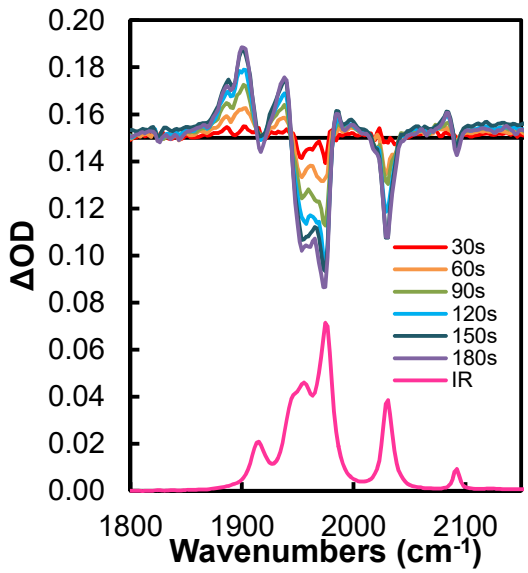

Figure 15. Long time UV-FTIR difference spectra for **1.**

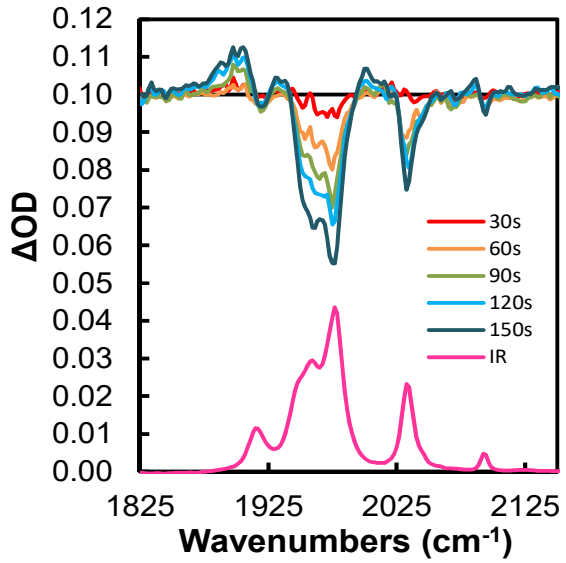

Figure 16. Long-time UV-FTIR difference spectra for **2.**

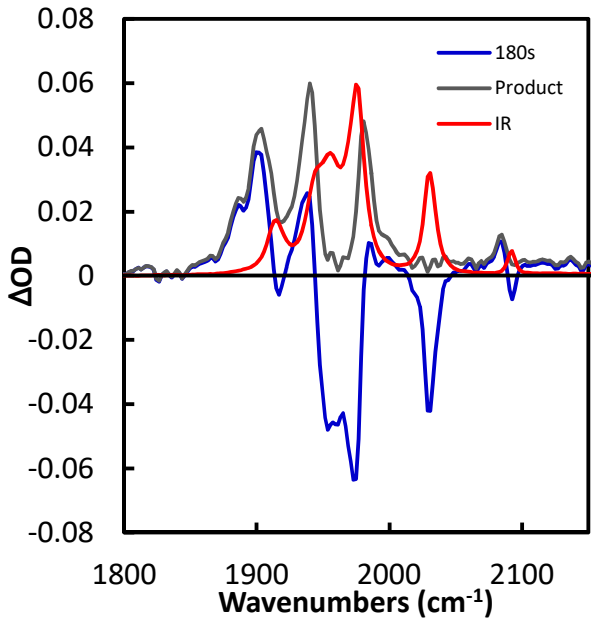

Figure 16. Long time product spectrum extrapolated from 180 s UV exposure and FTIR spectra for **1.**

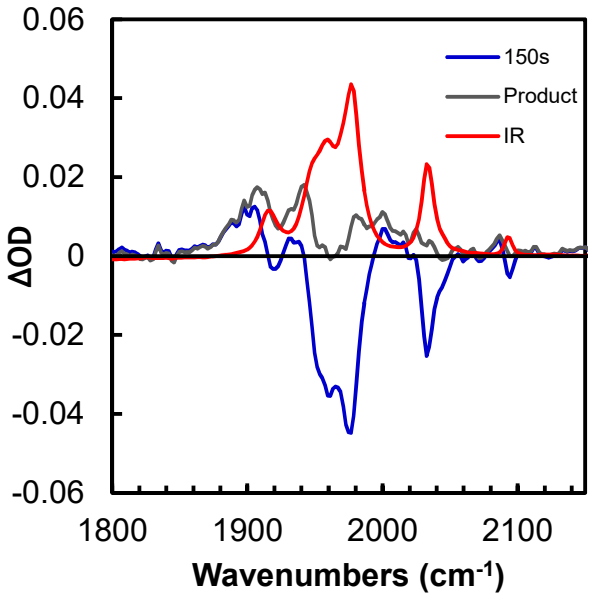

Figure 17. Long-time product spectrum extrapolated from 150 s UV exposure and FTIR spectra for **2**

Conclusions

The photodynamics of two asymmetric cyano-containing Fe-Fe hydrogenase model compounds were studied. Compound **1** was excited with 266 nm and 400 nm wavelengths while compound **2** was excited using only 400 nm pump. Picosecond photo-dynamics were examined using TRIR spectroscopy while stable product formation was investigated using UV-lamp exposure with FTIR difference spectroscopy.

Transient dynamics of bleaches and absorptions occur on two timescales. An initial 20-30 ps decay followed by a long-lived offset is observed for both compounds **1** and **2**. The 20-30 ps decay is the result of vibrational cooling and rotational dynamics. The long-lived offset suggests that one or more stable and soluble products are formed on the minute timescale. TRIR spectra were compared to DFT calculated spectra of different isomeric structures for each compound. This comparison indicated that the TRIR product spectra were not the result of isomerization, CO-loss, or CN-loss alone. Rather, the product spectra likely arise from a complex combination

of CO-loss and isomerization, which would be a nearly impossible product spectra to simulate. Identification of these products via further DFT modelling and NMR spectroscopy will be further explored.

References

(1) Adams, M. W. W. The Structure and Mechanism of Iron-Hydrogenases. *Biochim Biophys Acta. - Bioenergetics* **1990**, *1020* (2), 115–145.

(2) Adams, M. W. W.; Stiefel, E. I. BIOCHEMISTRY: Biological Hydrogen Production: Not So Elementary. *Science* **1998**, *282* (5395), 1842–1843.

(3) Adams, M. W.; Stiefel, E. L. Organomettalic Iron: The Key to Biological Hydrogen Meabolism. *Chem. Biol.* **2000**, *4*, 214–220.

(4) Bennett, B.; Lemon, B. J.; Peters, J. W. Reversible Cabon Monoxide Binding and Inhibition at the Active Site of the Fe-Only Hydrogenase. *Biochemistry* **2000**, *39*, 7455–7460.

(5) Hambourger, M.; Gervaldo, M.; Svedruzic, D.; King, P. W.; Gust, D.; Ghirardi, M.; Moore, A. L.; Moore, T. A. [FeFe]-Hydrogenase-Catalyzed H2 Production in a Photoelectrochemical Biofuel Cell. *J. Am. Chem. Soc.* **2008**, *130* (6), 2015–2022.

(6) Nicolet, Y.; Lemon, B. J.; Fontecilla-Camps, J. C.; Peters, J. W. A Novel FeS Cluster in Fe-Only Hydrogenases. *Trends Biochem. Sci.* **2000**, *25* (3), 138–142.

(7) Peters, J. W.; Lanzilotta, W. N.; Lemon, B. J.; Seefeldt, L. C. X-Ray Crystal Structure of the Fe-Only Hydrogenase (CpI) from Clostridium Pasteurianum to 1.8 Angstrom Resolution. *Science* **1998**, *282* (5395), 1853–1858.

(8) Tard, C.; Pickett, C. J. Structural and Functional Analogues of the Active Sites of the [Fe]-, [NiFe]-, and [FeFe]-Hydrogenases. *Chem. Rev.* **2009**, *109* (6), 2245–2274.

(9) Wang, X.-B.; Niu, S.; Yang, X.; Ibrahim, S. K.; Pickett, C. J.; Ichiye, T.; Wang, L.-S. Probing the Intrinsic Electronic Structure of the Cubane [4Fe-4S] Cluster, Nature's Favorite Cluster for Electron Transfer and Storage. *J. Am. Chem. Soc.* **2003**, *125*, 14072–14081.

(10) Gloaguen, F.; Lawrence, J. D.; Rauchfuss, T. B. Biomimetic Hydrogen Evolution Catalyzed by an Iron Carbonyl Thiolate. *J. Am. Chem. Soc.* **2001**, *123*, 9476–9477.

(11) Lubitz, W.; Ogata, H.; Rüdiger, O.; Reijerse, E. Hydrogenases. *Chemical Reviews* **2014**, *114* (8), 4081–4148.

(12) Siegbahn, P. E. M.; Tye, J. W.; Hall, M. B. Computational Studies of [NiFe] and [FeFe] Hydrogenases. *Chem. Rev.* **2007**, *107* (10), 4414–4435. https://doi.org/10.1021/cr050185y.

(13) Parkin, A. Understanding and Harnessing Hydrogenases, Biological Dihydrogen Catalysts; Metal Ions in Life Sciences; Springer, Dordrecht, 2014; Vol. 14, pp 99–124.

(14) Daraosheh, A. Q.; Harb, M. K.; Windhager, J.; Görls, H.; El-khateeb, M.; Weigand, W. Substitution Reactions at [FeFe] Hydrogenase Models Containing [2Fe3S] Assembly by Phosphine or Phosphite Ligands. *Organometallics* **2009**, *28* (21), 6275–6280.

(15) Gloaguen, F.; Lawrence, J. D.; Schmidt, M.; Wilson, S. R.; Rauchfuss, T. B. Synthetic and Structural Studies on [Fe2(SR)2(CN)x(CO)6-x]x- as Active Site Models for Fe-Only Hydrogenases. *J. Am. Chem. Soc.* **2001**, *123*, 12518–12527.

(16) Harb, M. K.; Apfel, U.-P.; KuÌˆbel, J.; GoÌˆrls, H.; Felton, G. A. N.; Sakamoto, T.; Evans, D. H.; Glass, R. S.; Lichtenberger, D. L.; El-khateeb, M.; Weigand, W. Preparation and Characterization of Homologous Diiron Dithiolato, Diselenato, and Ditellurato Complexes: [FeFe]-Hydrogenase Models. *Organometallics* **2009**, *28* (23), 6666–6675.
(17) Harb, M. K.; Niksch, T.; Windhager, J.; Görls, H.; Holze, R.; Lockett, L. T.; Okumura, N.; Evans, D. H.; Glass, R. S.; Lichtenberger, D. L.; El-khateeb, M.; Weigand, W. Synthesis and Characterization of Diiron Diselenolato Complexes Including Iron Hydrogenase Models. *Organometallics* **2009**, *28* (4), 1039–1048.
(18) Lawrence, J. D.; Li, H.; Rauchfuss, T. B. Beyond Fe-Only Hydrogenases: N-Functionalized 2-Aza-1,3-Dithiolates Fe2[(SCH2)2NR](CO)x (x = 5,6). *Chem. Commun.* **2001**, No. 16, 1482–1483.
(19) Le Cloirec, A.; Best, S. P.; Borg, S.; Davies, S. C.; Evans, D. J.; Jughes, D. L.; Pickett, C. J. A Di-Iron Dithiolate Possessing Structural Elements of the Carboyl/Cyande Sub-Site of the H-Centre of Fe-Only Hydrogenase. *Chem. Commun.* **1999**, 2285–2286.
(20) Lyon, E. J.; Georgakaki, I. P.; Reibenspies, J. H.; Darensbourg, M. Y. Coordination Sphere Flexibility of Active-Site Models for Fe-Only Hydrogenase: Studies in Intra- and Intermolecular Diatomic Ligand Exchange. *J. Am. Chem. Soc.* **2001**, *123*, 3268–3278.
(21) Song, L.-C.; Gao, W.; Feng, C.-P.; Wang, D.-F.; Hu, Q.-M. Investigations on Synthesis, Structure, and Properties of New Butterfly [2Fe2Se] Cluster Complexes Relevant to Active Sites of Some Hydrogenases. *Organometallics* **2009**, *28* (20), 6121–6130.
(22) Tye, J. W.; Darensbourg, M. Y.; Hall, M. B. De Novo Design of Synthetic Di-Iron(I) Complexes as Structural Models of the Reduced Form of Iron-Iron Hydrogenase. *Inorg. Chem.* **2006**, *45*, 1552–1559.
(23) Zhao, X.; Georgakaki, I. P.; Miller, M. L.; Yarbrough, J. C.; Darensbourg, M. Y. H/D Exchange Reactions in Dinuclear Iron Thiolates as Activity Assay Models of Fe−H2ase. *J. Am. Chem. Soc.* **2001**, *123* (39), 9710–9711.
(24) Zhao, X.; Georgakaki, I. P.; Miller, M. L.; Mejia-Rodriguez, R.; Chiang, C.-Y.; Darensbourg, M. Y. Catalysis of H2/D2 Scrambling and Other H/D Exchange Processes by [Fe]-Hydrogenase Model Complexes. *Inorg. Chem.* **2002**, *41*, 3917–3928.
(25) Nicolet, Y.; Piras, C.; Legrand, P.; Hatchikian, C. E.; Fontecilla-Camps, J. C. Desulfovibrio Desulfuricans Iron Hydrogenase: The Structure Shows Unusual Coordination to an Active Site Fe Binuclear Center. *Structure* **1999**, *7* (1), 13–23.
(26) Darensbourg, M. Y.; Lyon, E. J.; Zhao, X.; Georgakaki, I. P. The Organometallic Active Site of [Fe]Hydrogenase: Models and Entatic States. *Proc. Natl. Acad. Sci. U.S.A.* **2003**, *100* (7), 3683–3688. https://doi.org/10.1073/pnas.0536955100.
(27) Popescu, C. V.; Eckard, M. Electronic Structure of the H Cluster in [Fe]-Hydrogenases. *J. Am. Chem. Soc.* **1999**, *121*, 7877–7884.
(28) Ihara, M.; Nishihara, H.; Yoon, K.-S.; Lenz, O.; Friedrich, B.; Nakamoto, H.; Kojima, K.; Honma, D.; Kamachi, T.; Okura, I. Light-Driven Hydrogen Production by a Hybrid Complex of a [NiFe]-Hydrogenase and the Cyanobacterial Photosystem I. *Photochemistry and Photobiology* **2006**, *82* (3), 676–682.
(29) Lubner, C. E.; Grimme, R.; Bryant, D. A.; Golbeck, J. H. Wiring Photosystem I for Direct Solar Hydrogen Production. *Biochemistry* **2010**, *49* (3), 404–414.
(30) Fukuzumi, S.; Lee, Y.-M.; Nam, W. Thermal and Photocatalytic Production of Hydrogen with Earth-Abundant Metal Complexes. *Coordination Chemistry Reviews* **2018**, *355*, 54–73.

(31) Hongguang, C.; Mei, W.; Duan, L.; Licheng, S. Preparation, Characterization and Electrochemistry of an Iron-Only Hydrogenase Active Site Model Covalently Linked to a Ruthenium Tris(Bipyridine) Photosensitizer. *Journal of Coordination Chemistry* **2008**, *61* (12), 1856–1861.
(32) Sun, L.; Åkermark, B.; Ott, S. Iron Hydrogenase Active Site Mimics in Supramolecular Systems Aiming for Light-Driven Hydrogen Production. *Coord. Chem. Rev.* **2005**, *249* (15–16), 1653–1663.
(33) Wolpher, H.; Borgstrom, M.; Hammarstrom, L.; Bergquist, J.; Sundstrom, V.; Styring, S.; Sun, L.; Akermark, B. Synthesis and Properties of an Iron Hydrogenase Active Site Model Linked to a Ruthenium Tris-Bipyridine Photosensitizer. *Inorg. Chem. Commun.* **2003**, *6* (8), 989–991.
(34) Ott, S.; Kritikos, M.; Åkermark, B.; Sun, L. Synthesis and Structure of a Biomimetic Model of the Iron Hydrogenase Active Site Covalently Linked to a Ruthenium Photosensitizer. *Angew. Chem. Int. Ed.* **2003**, *42*, 3285–3288.
(35) Song, L. C.; Tang, M. Y.; Mei, S. Z.; Huang, J. H.; Hu, Q. M. The Active Site Model for Iron-Only Hydrogenases Coordinatively Bonded to a Metalloporphyrin Photosensitizer. *Organometallics* **2007**, *26* (7), 1575–1577.
(36) Song, L.-C.; Wang, L.-X.; Tang, M.-Y.; Li, C.-G.; Song, H.-B.; Hu, Q.-M. Synthesis, Structure, and Photoinduced Catalysis of [FeFe]-Hydrogenase Active Site Models Covalently Linked to a Porphyrin or Metalloporphyrin Moiety. *Organometallics* **2009**, *28* (13), 3834–3841.
(37) Ott, S.; Borgstrom, M.; Kritikos, M.; Lomoth, R.; Bergquist, J.; Åkermark, B.; Hammarstrom, L.; Sun, L. Model of the Iron Hydrogenase Active Site Covalently Linked to a Ruthenium Photosensitizer: Synthesis and Photophysical Properties. *Inorg. Chem.* **2004**, *43* (15), 4683–4692.
(38) Gao, S.; Huang, S.; Duan, Q.; Hou, J.; Jiang, D.; Liang, Q.; Zhao, J. Iron–Iron Hydrogenase Active Subunit Covalently Linking to Organic Chromophore for Light-Driven Hydrogen Evolution. *Int. J. Hydrogen Energy* **March 7**, *39* (20), 10434–10444.
(39) Gao, W.; Liu, J.; Jiang, W.; Wang, M.; Weng, L.; Åkermark, B.; Sun, L. An Azadithiolate Bridged Fe2S2 Complex as Active Site Model of FeFe-Hydrogenase Covalently Linked to a Re(CO)3(Bpy)(Py) Photosensitizer Aiming for Light-Driven Hydrogen Production. *C. R. Chim.* **2008**, *11* (8), 915–921.
(40) Ekström, J.; Abrahamsson, M.; Olson, C.; Bergquist, J.; Kaynak, F. B.; Eriksson, L.; Sun, L.; Becker, H.-C.; Åkermark, B.; Hammarström, L.; Ott, S. Bio-Inspired, Side-on Attachment of a Ruthenium Photosensitizer to an Iron Hydrogenase Active Site Model. *Dalton Trans.* **2006**, 4599–4606.
(41) Magnuson, A.; Anderlund, M.; Johansson, O.; Lindblad, P.; Lomoth, R.; Polivka, T.; Ott, S.; Stensjö, K.; Styring, S.; Sundström, V.; Hammarström, L. Biomimetic and Microbial Approaches to Solar Fuel Generation. *Acc. Chem. Res.* **2009**, *42* (12), 1899–1909.
(42) Stromberg, C. J.; Heilweil, E. J. Ultrafast Photodynamics of Cyano-Functionalized [FeFe] Hydrogenase Model Compounds. *The Journal Of Physical Chemistry. A* **2018**, *122* (16), 4023–4030.
(43) Bingaman, J. L.; Kohnhorst, C. L.; Van Meter, G. A.; McElroy, B. A.; Rakowski, E. A.; Caplins, B. W.; Gutowski, T. A.; Stromberg, C. J.; Webster, C. E.; Heilweil, E. J. Time-Resolved Vibrational Spectroscopy of [FeFe]-Hydrogenase Model Compounds. *J. Phys. Chem. A* **2012**, *116* (27), 7261–7271.

(44) Johnson, M.; Thuman, J.; Letterman, R. G.; Stromberg, C. J.; Webster, C. E.; Heilweil, E. J. Time-Resolved Infrared Studies of a Trimethylphosphine Model Derivative of [FeFe]-Hydrogenase. *J. Phys. Chem. B* **2013**, *117* (49), 15792–15803.
(45) Meyer, R. L.; Zhandosova, A. D.; Biser, T. M.; Heilweil, E. J.; Stromberg, C. J. Photochemical Dynamics of a Trimethyl-Phosphine Derivatized [FeFe]-Hydrogenase Model Compound. *Chemical Physics* **2018**, *512*, 135–145.
(46) Thornley, W.; Wirick, S. A.; Riedel-Topper, M.; DeYonker, N. J.; Bitterwolf, T. E.; Stromberg, C. J.; Heilweil, E. J. Photodynamics of [FeFe]-Hydrogenase Model Compounds with Bidentate Heterocyclic Ligands. *J. Phys. Chem. B* **2019**, *123* (33), 7137–7148.
(47) Kania, R.; Frederix, P. W. J. M.; Wright, J. A.; Ulijn, R. V.; Pickett, C. J.; Hunt, N. T. Solution-Phase Photochemistry of a [FeFe]Hydrogenase Model Compound: Evidence of Photoinduced Isomerisation. *J. Chem. Phys.* **2012**, *136* (4), 044521–044529.
(48) Kaziannis, S.; Santabarbara, S.; Wright, J. A.; Greetham, G. M.; Towrie, M.; Parker, A. W.; Pickett, C. J.; Hunt, N. T. Femtosecond to Microsecond Photochemistry of a [FeFe]Hydrogenase Enzyme Model Compound. *J. Phys. Chem. B* **2010**, *114* (46), 15370–15379.
(49) Caplins, B. W.; Lomont, J. P.; Nguyen, S. C.; Harris, C. B. Vibrational Cooling Dynamics of a [FeFe]-Hydrogenase Mimic Probed by Time-Resolved Infrared Spectroscopy. *The Journal of Physical Chemistry A* **2014**, *118* (49), 11529–11540.
(50) Frederix, P. W. J. M.; Adamczyk, K.; Wright, J. A.; Tuttle, T.; Ulijn, R. V.; Pickett, C. J.; Hunt, N. T. Investigation of the Ultrafast Dynamics Occurring during Unsensitized Photocatalytic H2 Evolution by an [FeFe]-Hydrogenase Subsite Analogue. *Organometallics* **2014**, *33* (20), 5888–5896.
(51) Certain Commercial Equipment, Instruments, or Materials Are Identified in This Paper to Foster Understanding. Such Identification Does Not Imply Recommendation or Endorsement by the National Institute of Standards and Technology, nor Does It Imply That the Materials or Equipment Identified Are Necessarily the Best Available for the Purpose.
(52) Parr, R. G.; Yang, W. *Density-Functional Theory of Atoms and Molecules*; Oxford University Press: New York, 1989.
(53) Frisch, M. J.; Trucks, G. W.; Schlegel, H. B.; Scuseria, G. E.; Robb, M. A.; Cheeseman, J. R.; Scalmani, G.; Barone, V.; Mennucci, B.; Petersson, G. A.; Nakatsuji, H.; Caricato, M.; Li, X.; Hratchian, H. P.; Izmaylov, A. F.; Bloino, J.; Zheng, G.; Sonnenberg, J. L.; Hada, M.; Ehara, M.; Toyota, K.; Fukuda, R.; Hasegawa, J.; Ishida, M.; Nakajima, T.; Honda, Y.; Kitao, O.; Nakai, H.; Vreven, T.; Montgomery, J. A.; Peralta, J. E.; Ogliaro, F.; Bearpark, M.; Heyd, J. J.; Brothers, E.; Kudin, K. N.; Staroverov, V. N.; Kobayashi, R.; Normand, J.; Raghavachari, K.; Rendell, A.; Burant, J. C.; Iyengar, S. S.; Tomasi, J.; Cossi, M.; Rega, N.; Millam, J. M.; Klene, M.; Knox, J. E.; Cross, J. B.; Bakken, V.; Adamo, C.; Jaramillo, J.; Gomperts, R.; Stratmann, R. E.; Yazyev, O.; Austin, A. J.; Cammi, R.; Pomelli, C.; Ochterski, J. W.; Martin, R. L.; Morokuma, K.; Zakrzewski, V. G.; Voth, G. A.; Salvador, P.; Dannenberg, J. J.; Dapprich, S.; Daniels, A. D.; Farkas, O.; Foresman, J. B.; Ortiz, J. V.; Cioslowski, J.; Fox, D. J. *Gaussian 09 Revision A.02*; Gaussian Inc.: Wallingford, CT, 2009.
(54) Becke, A. D. Density-Functional Exchange-Energy Approximation with Correct Asymptotic Behavior. *Phys. Rev. A* **1988**, *38* (6), 3098–3100.

(55) Perdew, J. P. Erratum: Density-Functional Approximation for the Correlation Energy of the Inhomogeneous Electron Gas. *Phys. Rev. B* **1986**, *34* (10), 7406–7406.
(56) Perdew, J. P. Density-Functional Approximation for the Correlation Energy of the Inhomogeneous Electron Gas. *Phys. Rev. B* **1986**, *33* (12), 8822–8824.
(57) Schafer, A.; Huber, C.; Ahlrichs, R. Fully Optimized Contracted Gaussian Basis Sets of Triple Zeta Valence Quality for Atoms Li to Kr. *J. Chem. Phys.* **1994**, *100* (8), 5829–5835.
(58) Schafer, A.; Horn, H.; Ahlrichs, R. Fully Optimized Contracted Gaussian Basis Sets for Atoms Li to Kr. *J. Chem. Phys.* **1992**, *97* (4), 2571–2577.
(59) Ridley, A. R.; Stewart, A. I.; Adamczyk, K.; Ghosh, H. N.; Kerkeni, B.; Guo, Z. X.; Nibbering, E. T. J.; Pickett, C. J.; Hunt, N. T. Multiple-Timescale Photoreactivity of a Model Compound Related to the Active Site of [FeFe]-Hydrogenase. *Inorg. Chem.* **2008**, *47* (17), 7453–7455.
(60) Stewart, A. I.; Clark, I. P.; Towrie, M.; Ibrahim, S. K.; Parker, A. W.; Pickett, C. J.; Hunt, N. T. Structure and Vibrational Dynamics of Model Compounds of the [FeFe]-Hydrogenase Enzyme System via Ultrafast Two-Dimensional Infrared Spectroscopy. *J. Phys. Chem. B* **2008**, *112* (32), 10023–10032.
(61) Stewart, A. I.; Wright, J. A.; Greetham, G. M.; Kaziannis, S.; Santabarbara, S.; Towrie, M.; Parker, A. W.; Pickett, C. J.; Hunt, N. T. Determination of the Photolysis Products of [FeFe]Hydrogenase Enzyme Model Systems Using Ultrafast Multidimensional Infrared Spectroscopy. *Inorg. Chem.* **2010**, *49* (20), 9563–9573.